

HYBRID METHODS FOR SIMULATION
OF MUON IONIZATION COOLING CHANNELS

BY
JOSIAH D. KUNZ

Submitted in partial fulfillment of the
requirements for the degree of
Doctor of Philosophy in Physics
in the Graduate College of the
Illinois Institute of Technology

Approved _____
Advisor

Chicago, Illinois
August 2016

DMK comments

Mostly quite good
clearly written

Some more justification
of the math would help,
and some more details
could be omitted

Some stylistic issues.

ACKNOWLEDGMENT

It goes without saying that I am grateful to God, who has guided me in my academic path and has allowed me to fulfil my dream of getting my Ph.D. in Physics. I would also like to thank my wife, Meredith Kunz, who has been by my side even before graduate school. I am very fortunate to have an advisor like Pavel Snopok, who puts in so much time and thought on my behalf. Pavel has worked with me on every turn. I could be no luckier than to have an advisor like him.

I would like to acknowledge the committee for their valuable time and selflessness: Dan Kaplan, Linda Spentzouris, Yagmur Torun, and Xiaofan Li. The Department of Energy is also acknowledged for funding me through Pavel.

On a less serious note, I would like to thank my late cat Scout, who slept on my lap through many of my COSY days. Although he did not make it to see the end result, he will not be forgotten. I would also like to thank my puppy Oliver for his patience with me while writing my thesis, and for keeping my mind fresh with breaks for playtime.

TABLE OF CONTENTS

| | Page |
|--|------|
| ACKNOWLEDGEMENT | iii |
| LIST OF TABLES | vi |
| LIST OF FIGURES | ix |
| LIST OF SYMBOLS | x |
| ABSTRACT | xiv |
| CHAPTER | |
| 1. INTRODUCTION | 1 |
| 1.1. Muon-based Accelerators | 1 |
| 1.2. COSY Infinity | 3 |
| 1.3. Introduction to Matter-Dominated Lattices | 8 |
| 1.4. Emittance | 13 |
| 1.5. Looking Forward | 17 |
| 2. STOCHASTIC PROCESSES IN OTHER CODES | 20 |
| 2.1. Energy Straggling in ICOOL | 20 |
| 2.2. Multiple Scattering in ICOOL | 35 |
| 2.3. Energy Straggling in G4Beamline | 43 |
| 2.4. Multiple Scattering in G4Beamline | 47 |
| 3. STOCHASTIC PROCESSES IN COSY INFINITY | 53 |
| 3.1. Energy Straggling in COSY | 53 |
| 3.2. Multiple Scattering in COSY Infinity | 56 |
| 3.3. Transverse Displacement in COSY Infinity | 65 |
| 3.4. Temporal Displacement in COSY Infinity | 69 |
| 4. SOFTWARE IMPLEMENTATION | 72 |
| 4.1. User Input | 72 |
| 4.2. COSYScript Level | 74 |
| 4.3. FORTRAN Level | 75 |
| 4.4. Summary | 76 |
| 5. RESULTS | 77 |
| 5.1. Benchmark Against Other Codes | 77 |
| 5.2. Validation | 90 |

| | |
|---|-----|
| 5.3. The Muon Ionization Cooling Experiment | 93 |
| 5.4. Summary | 105 |
| APPENDIX | 105 |
| A. DERIVATION OF TRANSVERSE EMITTANCE | 106 |
| B. DERIVATION OF IMPLEMENTED SCATTERING CROSS SECTION | 111 |
| C. A BRIEF REVIEW OF RELEVANT PARTICLE PHYSICS | 123 |
| D. EXPLICIT FORMS OF THE DIRAC GAMMA MATRICES AND PAULI MATRICES | 127 |
| E. PROOFS OF USEFUL DIRAC GAMMA MATRIX TRACE IDENTITIES | 129 |
| E.1. Proof of $(\gamma^5)^2 = I_4$ | 130 |
| E.2. Proof of $\gamma^5 \gamma^\alpha = -\gamma^\alpha \gamma^5$ | 130 |
| E.3. Proof of $\text{Tr}(\text{odd number of } \gamma \text{ matrices}) = 0$ | 131 |
| E.4. Proof of $\text{Tr}(\gamma^\alpha \gamma^\beta) = 4\eta^{\alpha\beta}$ | 132 |
| E.5. Proof of $\text{Tr}(\gamma^\alpha \gamma^\beta \gamma^\delta \gamma^\epsilon) = 4(\eta^{\alpha\beta} \eta^{\delta\epsilon} - \eta^{\alpha\delta} \eta^{\beta\epsilon} + \eta^{\alpha\epsilon} \eta^{\beta\delta})$ | 133 |
| F. REPRODUCTION OF IMPLEMENTED CODE | 134 |
| F.1. Example COSY Deck using ABSPOLY | 135 |
| F.2. COSYScript | 140 |
| F.3. FORTRAN | 151 |
| BIBLIOGRAPHY | 188 |

LIST OF TABLES

| Table | Page |
|---|------|
| 1.1 Energy loss table for muons in iron. | 18 |
| 2.1 G4Beamline scattering distribution parameters. | 49 |
| 5.1 MICE Step IV coil parameters. | 95 |
| 5.2 MICE Step IV initial distribution Gaussian parameters. | 95 |
| 5.3 Run times for MICE Step IV simulation. | 99 |
| 5.4 Step size dependence for the absorber-coil section of MICE Step IV lattice for liquid hydrogen. | 101 |
| 5.5 Step size dependence for MICE Step IV lattice. | 104 |

LIST OF FIGURES

| Figure | | Page |
|--------|--|------|
| 1.1 | The current model of particle physics. | 1 |
| 1.2 | The reference orbit. | 5 |
| 1.3 | Example of some map \mathcal{M} creating a bijection from s_0 to s_1 | 7 |
| 1.4 | Example of two maps $\mathcal{M}(s_0, s_1)$ and $\mathcal{M}(s_1, s_2)$. These two maps may be combined together to reduce to a single map, $\mathcal{M}(s_0, s_2)$. . | 7 |
| 1.5 | Classical muon-target interaction model. | 8 |
| 1.6 | Quantum muon-target interaction model. | 9 |
| 1.7 | Proposed muon accelerator schematics. | 11 |
| 1.8 | Cartoon of a cooling channel. | 12 |
| 1.9 | Vector diagram illustrating the principle of ionization cooling in Figure 1.8. | 13 |
| 1.10 | x - θ phase space examples. | 14 |
| 1.11 | Stopping power curve for antimuons on copper. | 17 |
| 2.1 | Classical model of particle passage through matter. | 23 |
| 2.2 | Plot of $\int w(u)(1 - e^{-pu}) du$ | 32 |
| 2.3 | Example of the Landau function. | 34 |
| 2.4 | Quantum scattering model. | 37 |
| 2.5 | Two parts of Green's function with their poles at $s = \pm k$, altered to be closed by a semicircle at $ s = \pm\infty$ | 40 |
| 3.1 | λ_{max} vs. $\langle\lambda\rangle$ over a variety of liquid hydrogen absorber lengths and initial beam momenta. | 55 |
| 3.2 | Example of the COSY cumulative angular distribution function. . | 59 |
| 3.3 | Example of the first iteration of the COSY CDF algorithm. . . . | 61 |
| 3.4 | Example of a muon entering an absorber with some nonzero initial angle. | 63 |
| 3.5 | Two examples of true paths. | 66 |

| | | |
|------|--|----|
| 3.6 | 2D histogram of (x, p_x) phase space. | 67 |
| 3.7 | Cross section of Figure 3.6 at $p_x = 0.08$ keV/c. | 68 |
| 3.8 | Phase space portrait of Figure 3.6. | 69 |
| 3.9 | Sample simulation results for the implementation of the transverse coordinate correction algorithm. | 69 |
| 3.10 | Sample simulation results for the implementation of the temporal displacement algorithm discussed in this section. | 71 |
| 4.1 | A flowchart for the structure of the new COSY routines implemented in this work. | 73 |
| 4.2 | Cartoon example of some of the ABSPOLY parameters. | 74 |
| 5.1 | Muons of momentum 100 MeV/c through 1 mm liquid hydrogen. . | 78 |
| 5.2 | Muons of momentum 100 MeV/c through 10 mm liquid hydrogen. . | 79 |
| 5.3 | Muons of momentum 100 MeV/c through 100 mm liquid hydrogen. . | 80 |
| 5.4 | Muons of momentum 200 MeV/c through 1 mm liquid hydrogen. . | 81 |
| 5.5 | Muons of momentum 200 MeV/c through 10 mm liquid hydrogen. . | 82 |
| 5.6 | Muons of momentum 200 MeV/c through 100 mm liquid hydrogen. . | 83 |
| 5.7 | Muons of momentum 300 MeV/c through 1 mm liquid hydrogen. . | 84 |
| 5.8 | Muons of momentum 300 MeV/c through 10 mm liquid hydrogen. . | 85 |
| 5.9 | Muons of momentum 300 MeV/c through 100 mm liquid hydrogen. . | 86 |
| 5.10 | Muons of momentum 400 MeV/c through 1 mm liquid hydrogen. . | 87 |
| 5.11 | Muons of momentum 400 MeV/c through 10 mm liquid hydrogen. . | 88 |
| 5.12 | Muons of momentum 400 MeV/c through 100 mm liquid hydrogen. . | 89 |
| 5.13 | MuScat angular scattering results for 109 mm of liquid hydrogen compared against COSY (red), G4BL (green), and ICOOL (blue). . | 91 |
| 5.14 | MuScat angular scattering results for 159 mm of liquid hydrogen compared against COSY (red), G4BL (green), and ICOOL (blue). . | 92 |
| 5.15 | MuScat angular scattering results for 3.73 mm of beryllium compared against COSY (red), G4BL (green), and ICOOL (blue). . . | 93 |
| 5.16 | MICE Step IV cell. | 94 |

| | | |
|------|--|-----|
| 5.17 | MICE Step IV x position results for 350 mm of liquid hydrogen. . . | 97 |
| 5.18 | MICE Step IV x angle results for 350 mm of liquid hydrogen. . . . | 97 |
| 5.19 | MICE Step IV final energy results for 350 mm of liquid hydrogen. . . | 98 |
| 5.20 | MICE Step IV x position results for 65 mm of lithium hydride. . . | 99 |
| 5.21 | MICE Step IV x angle results for 65 mm of lithium hydride. . . . | 100 |
| 5.22 | MICE Step IV final energy results for 65 mm of lithium hydride. . . | 100 |
| 5.23 | Absorber-coil simulation results for x with 10^5 muons and a 5 step propagation. | 102 |
| 5.24 | Absorber-coil simulation results for θ_x with 10^5 muons and a 5 step propagation. | 102 |
| 5.25 | Absorber-coil simulation results for the final energy with 10^5 muons and a 5 step propagation. | 103 |
| 5.26 | MICE simulation results for x with 10^5 muons at 5th order and 50 steps. | 104 |
| 5.27 | MICE simulation results for θ_x with 10^5 muons at 5th order and 50 steps. | 105 |
| A.1 | Sample scatterplot of a bivariate Gaussian with its projected ellipse. . | 109 |
| B.1 | Feynman diagram for electron-muon scattering. | 113 |
| B.2 | Mathematical interpretation the three branches of the Feynman di- agram in Figure B.1. | 114 |
| B.3 | COSY treatment of muon-electron scattering. | 121 |

LIST OF SYMBOLS

| Symbol | Definition |
|----------------------------|--|
| \mathcal{A}, \mathcal{B} | Matrix, general |
| a, b_r, d_r, p_g, q_g | GEANT4 angular parameters |
| b | Impact parameter |
| b_c | COSY offset of scattering tail |
| C, C_i | Normalization constant; shell correction parameter) |
| C_{Euler} | Euler's constant (≈ 0.577) |
| c | Speed of light in a vacuum |
| $\langle dE/dx \rangle$ | Energy loss per unit length, mean (Bethe Bloch) |
| E | Energy (general; context dependent) |
| e | Fundamental charge (such that $z_{ch} = eQ$) |
| e^-, e^+ | Electron or antielectron |
| F | Distribution function antiderivative (general; context depen- dent) |
| f | Distribution function (general; context dependent) |
| f_i | Oscillator strengths |
| $g(E)$ | Energy loss distribution function |
| $g(u)$ | Angular distribution function |
| H | Distribution function antiderivative (general; context depen- dent) |
| h | Distribution function (general; context dependent); Planck's constant |
| h_i | Highland corrections ($i = 1, 2$) |

| | |
|-------------------|---|
| \hbar | Planck's constant divided by 2π |
| I | Ionization energy (mean) |
| I_j | Unit matrix of rank j |
| K, K_i | Constant (context dependent) |
| L | Length (of absorber or step size) |
| ℓ | Time-of-flight in units of length (COSY coordinate) |
| M | Moments of a function |
| \mathcal{M} | Scattering amplitude; transfer map |
| m | Mass (general; context dependent) |
| m_e | Electron mass |
| m_μ | Muon mass |
| N | Atomic density |
| N_A | Avagadro's Number |
| N_{el} | Electron density |
| P | Four-momentum |
| P_k | Legendre polynomials |
| p | Momentum (total) |
| (p_x, p_y, p_z) | Beamline momentum coordinate system |
| Q_i | Charge number of particle i |
| r_e | Electron radius |
| s | Arc length coordinate |
| T | Transverse coordinate |

| | |
|-----------------|---|
| T_{max} | Maximum transferrable kinetic energy |
| t | Time (variable) |
| t_z | True path length |
| U | Spinor |
| u | Angular cosine variable ($u = \cos \theta$); dummy variable |
| u_0 | Characteristic cosine variable |
| \vec{v} | Unit vector |
| v | Velocity |
| w | Weight for a distribution function (context dependent) |
| X_0 | Radiation length |
| (x, y, z) | Beamline position coordinate system |
| Z | Atomic charge |
| z_{ch} | Electric charge |
| z_g | Geometric path length |
| α | Dummy variable |
| β | Relativistic velocity ($\beta = v/c$) |
| γ | Lorentz factor |
| γ^α | Dirac gamma matrix |
| δ | Density correction parameter; Dirac function |
| ϵ | Energy loss fluctuation ($\epsilon = \Delta E$); emittance |
| ζ | COSY amplitude of scattering tail |

| | |
|----------------------|--|
| η | Minkowski metric |
| θ | Scattered angle |
| θ_0 | Angular distribution Gaussian width |
| κ | Vavilov limit parameter |
| λ | Landau parameter |
| λ_k | Transport free mean paths, k^{th} value |
| λ_v | Vavilov parameter |
| μ | Mean; muon |
| $\nu_e, \bar{\nu}_e$ | Electron neutrino or electron antineutrino |
| ν_μ | Muon neutrino |
| π | Circle constant |
| ρ | Density |
| Σ | Cross section |
| σ | Standard deviation |
| σ^j | Pauli matrices |
| ϕ | Laplace transformed function |
| ψ | Wavefunction, time-independent component |
| Ω | Solid angle |
| $*$ | Complex conjugate |
| \dagger | Transpose conjugate |
| T | Transpose of a matrix |

ABSTRACT

COSY Infinity is an arbitrary-order beam dynamics simulation and analysis code. It can determine high-order transfer maps of combinations of particle optical elements of arbitrary field configurations. For precision modeling, design, and optimization of next-generation muon beam facilities, its features make it a very attractive code. New features are being developed for inclusion in COSY to follow the distribution of charged particles through matter. To study in detail some of the properties of muons passing through material, the transfer map approach alone is not sufficient. The interplay of beam optics and atomic processes must be studied by a hybrid transfer map–Monte Carlo approach in which transfer map methods describe the average behavior of the particles in the accelerator channel including energy loss, and Monte Carlo methods are used to provide small corrections to the predictions of the transfer map accounting for the stochastic nature of scattering and straggling of particles. The advantage of the new approach is that it is very efficient in that the vast majority of the dynamics is represented by fast application of the high-order transfer map of an entire element and accumulated stochastic effects as well as possible particle decay. The gains in speed shown in this work are expected to simplify the optimization of muon cooling channels which are usually very computationally demanding due to the need to repeatedly run large numbers of particles through large numbers of configurations. This work describes the development of the required algorithms and their application to the simulation of muon ionization cooling channels. The code is benchmarked against other codes, validated with experimental results, and predicts results for current muon ionization cooling efforts.

CHAPTER 1 INTRODUCTION

1.1 Muon-based Accelerators

Muons (μ) were first discovered experimentally in 1947 by Powell *et al* [1] who were looking for the Yukawa meson. It is now known that muons fit into a particle group called leptons, and fit into the standard model (along with other fundamental particles) as shown in Figure 1.

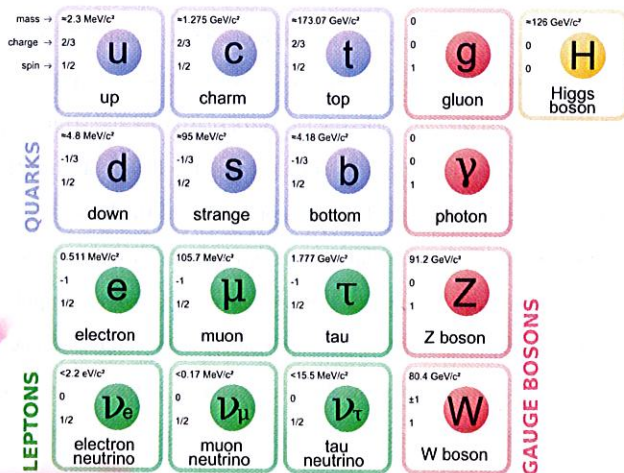


Figure 1.1: The current model of particle physics. Image courtesy of [2].

Similar to the electron (e), the muon carries a fundamental charge of ± 1 , a total spin of $1/2$, and observes the electromagnetic and weak forces. Moreover, the muon also has a corresponding neutrino: the muon neutrino (ν_μ). However, the muon (mass = $105.7 \text{ MeV}/c^2$) is about 200 times heavier than the electron (mass = 0.511

MeV/c^2). Indeed, sometimes it is useful to think of a muon simply as a heavy electron, but the mass implies several unique characteristics. One of these is the instability of muons, and results in muons decaying into an electron, an electron antineutrino, and a muon neutrino:

$$\mu \rightarrow e + \bar{\nu}_e + \nu_\mu.$$

This is quite interesting, as it means muons are a double-edged sword. On the one hand, their point-like nature means that the muon collisions are clean. That is to say, muon colliders have a great advantage over, e.g., proton colliders since protons are composed of three quarks. Each quark may have a different flavor or energy level and hence adds more variables to the analysis. Furthermore, each quark is bound and so gluon interactions must also be considered. These quarks and gluons may undergo hadronization when interacting with one another, creating a plethora of possible hadrons. Hadronization is not fully understood, and so these sprays of hadrons are typically lumped together as a single "jet". While there are many working models for jet analysis, none are exact. Conversely, any data from muon interactions will have relatively little noise and will not produce jets.

Clean collisions can also be achieved with linear electron colliders. Yet unlike the electron, the muon does not emit a large amount of synchrotron radiation as it is accelerated. This is because the power irradiated off a particle due to synchrotron radiation is inversely proportional to the mass of the particle to the fourth power [3]:

$$P \propto 1/m^4.$$

Therefore, the relative power loss due to synchrotron radiation for electrons and muons is $P_e/P_\mu \propto m_\mu^4/m_e^4 \approx 1.8 \times 10^9$. Since muons lose power via synchrotron radiation at roughly one-billionth the rate of electrons, it is possible to have a circular muon accelerator. Furthermore, due to the small mass of a muon compared to a proton

should use human rather than computer notation

also possible for electrons \Rightarrow much more quantitative discussion

($\sim 105 \text{ MeV}/c^2$ vs. $\sim 938 \text{ MeV}/c^2$), muons are easier to accelerate. This means that a muon facility can be much smaller than its proton counterpart.

Wrong reason

this work is

However, there is one problem with a muon accelerator. A rest frame lifetime of $2 \mu\text{s}$ requires the muons to be accelerated quickly before they decay. This is a challenge for circular colliders which require a high-intensity beam.

that

Overall, it appears that there are several advantages and one key disadvantage: the $2 \mu\text{s}$ mean rest frame lifetime of the muon. However, this is only a disadvantage for muon colliders. Another application, which turns the moderately short lifetime into an advantage, is a neutrino factory. This is a facility that is dedicated to the output of a neutrino beam. Muons have two primary advantages over fission reactor neutrino sources. The first is that muons decay into exactly two flavors of neutrino: electron and muon. Therefore, the initial composition of the neutrino beam would be well-defined. This is important since neutrinos can change their flavors over time. Secondly, since neutrinos have no electric charge, they cannot be manipulated via electromagnetic focusing methods. However, the beam of muons can be focused into a high-intensity beam, and the intensity of the neutrino beam will reflect this.

Wrong comparison produce only 2e (assumed small)

Also true of $\pi^\pm \Rightarrow$ but to be a bit more quantitative

1.2 COSY Infinity

COSY Infinity is a beamline simulation tool used in the design, analysis, and optimization of particle accelerators [4]. COSY uses the transfer map approach, which evaluates the overall effect of a system on a beam of particles using differential algebra. This involves expanding an ordinary differential equation into multivariate Taylor polynomials up to arbitrary order [5]. Each particle in this work is represented by its coordinates as a phase space vector. The form of phase space vectors used in

of what?
is what?

$$\mathbf{Z} = \begin{pmatrix} x \\ y \\ l = k(t - t_0) \\ a = p_x/p_0 \\ b = p_y/p_0 \\ \delta = (E - E_0)/E_0 \end{pmatrix}, \quad (1.1)$$

where the coordinates are transverse positions (x, y), time-of-flight in units of length (l), transverse angles w.r.t. the reference particle (a, b), and kinetic energy deviations w.r.t. the reference particle (δ). The 0 subscript in the definitions denotes the reference particle properties.

In beam physics, phase space vectors \mathbf{Z} are subject to physics processes. This subjugation can usually be represented by a differential equation. For example, a particle in an electric field is subject to the force law [3]

$$\mathbf{F} = Q(\mathbf{E} + \mathbf{v} \times \mathbf{B}),$$

or in terms of the momentum,

$$\frac{d}{dt}\mathbf{p} = Q(\mathbf{E} + \frac{1}{m}\mathbf{p} \times \mathbf{B}).$$

non-relativistic?

Fortunately, any phase space vector \mathbf{Z} in an arbitrary order ordinary differential equation (ODE) can be rewritten as a first-order ODE [5]. For an order n ODE, a first-order ODE is constructed by introducing $n - 1$ new variables. This is to say that

$$\frac{d^n}{dt^n}\mathbf{Z} = \mathbf{f}\left(\frac{d^0}{dt^0}\mathbf{Z}, \dots, \frac{d^{n-1}}{dt^{n-1}}\mathbf{Z}\right)$$

use 11084, 11085

can be rewritten as

$$\frac{d}{dt} \begin{pmatrix} Z \\ Z_1 \\ \vdots \\ Z_{n-1} \end{pmatrix} = \begin{pmatrix} Z_1 \\ Z_2 \\ \vdots \\ f(Z, \dots, Z_{n-1}) \end{pmatrix}.$$

Here, f represents the physics processes. For the Maxwell's equations example, the equation is already first order in a and b , with the momentum component of f as

$$f(\mathbf{p}) = Q(\mathbf{E} + \frac{1}{m}\mathbf{p} \times \mathbf{B}) = Q(\mathbf{E} + \frac{1}{m}[ap_0\hat{x} + bp_0\hat{y} + p_z\hat{z}] \times \mathbf{B}).$$

Furthermore, COSY does not use time as the independent variable, but rather arc length s (see Figure 1.2).



Figure 1.2: The reference orbit. Figure courtesy of [6].

If there exists a unique evolution of \mathbf{Z} then it is possible to construct the so-called transfer map \mathcal{M} . Mathematically, this relationship is $\mathbf{Z}(s) = \mathcal{M}(s_0, s) * \mathbf{Z}(s_0)$, with $*$ representing the application of the transfer map to the phase space vector \mathbf{Z} at s_0 .

It is possible to construct a transfer map for most cases in beamline physics. This is because most beamline elements follow differential equations which yield unique solutions dependent on initial conditions (such as Maxwell's equations). If there does not exist a unique evolution of \mathbf{Z} then it is not possible to construct the

transfer map. Systems which produce a unique evolution of \mathbf{Z} are called "deterministic".

An example of the relationship between the initial phase space vector, the transfer map, and the final phase space vector can be seen in Figure 1.3. The initial phase space occupied by the beam of particles is at the coordinate s_0 . Physically, there exists some deterministic beamline element between s_0 and s_1 . This element can be represented by the map \mathcal{M} , which creates a bijection for the phase space vectors $\mathbf{Z}(s_0)$ and $\mathbf{Z}(s_1)$ between the initial coordinate s_0 and the final coordinate s_1 .

Entire lattices may also be represented by a single transfer map. This is done by dividing the lattice into its base components or elements. A transfer map for each corresponding element may then be produced. For two example elements between coordinates s_0 and s_2 (see Figure 1.4), the composition of two maps yields another map: $\mathcal{M}(s_1, s_2) \times \mathcal{M}(s_0, s_1) = \mathcal{M}(s_0, s_2)$. Therefore, it is possible to simplify the middle part s_1 . In this way, the transfer maps from small components build up into a single transfer map for the whole system. Computationally this is advantageous because once calculated, it is much faster to apply a single transfer map to a distribution of particles than to simulate that same distribution through many meters of individual lattice elements.

Along with the tracking of particles through a lattice, COSY also has a plethora of analysis and optimization tools, including (but not limited to) lattice aberration and correction tools, support for Twiss parameters, support for tunes and nonlinear tune shifts, built-in optimizers for lattice design, and spin tracking.

Valid elements are any beamline elements that are deterministic. Elements used in this study are magnetic multipoles (dipoles, quadrupoles, etc.), solenoidal coils, radiofrequency (RF) cavities, and drifts. Currently supported elements in COSY